Photometric measurements of geostationary satellites over the Western Pacific Region

Jovan Skuljan
Defence Technology Agency, Auckland, New Zealand

ABSTRACT

The Defence Technology Agency (DTA) operates a small space situational awareness (SSA) observatory at the tip of Whangaparaoa Peninsula, north of Auckland, New Zealand. The observatory is equipped with two 11-inch instruments: an f/10 Schmidt–Cassegrain telescope and an f/2.2 Rowe-Ackermann Schmidt astrograph, on a Paramount MEII robotic telescope mount. The imaging equipment includes two FLI ML11002 cooled CCD cameras, as well as two smaller QSI 640ws detectors. In addition, a specialised quadruple polarimetric camera (QuadCam) was recently built for polarimetric observations. The observatory is currently being modified to support fully automated and/or remotely controlled operation for more efficient data collection.

Over the past several months the equipment was mainly used on geostationary satellites. A number of objects over the Western Pacific Region were observed in order to test the equipment and data reduction procedures, as well as to estimate the overall precision of astrometric and photometric measurements. It was found that high-quality data could be obtained for satellites as low as 5-10 degrees above the horizon, so that the total coverage of the equatorial belt extends to about 140 degrees. This includes all objects with eastern longitudes above 105 degrees and western longitudes above 115 degrees.

The latest GAIA catalogue from the European Space Agency (ESA) was used for the calibration of satellite images. The photometric calibration using the GAIA G-band magnitudes gives a typical uncertainty of about 0.1 magnitudes, based on 100-200 stars. The magnitude limit of our system is estimated to be about 15-16, depending on the exposure duration (20-60 seconds). The random error (standard deviation) in photometry is usually less than 0.01. The start and finish of every exposure is timed to a high accuracy of better than 1 millisecond, using a specialised GPS unit.

The measurements collected so far demonstrate that our equipment is capable of monitoring relatively faint objects (15-16 magnitude) in the geostationary belt. The high quality photometric data can be used to study any anomalies in the behaviour of the satellite, such as, for example, change in orientation and uncontrolled spin.

1. INTRODUCTION

Over the past several years, there has been a steady increase in the space situational awareness (SSA) capability at the Defence Technology Agency (DTA) and within the New Zealand Defence Force (NZDF). The development started with the preparations for the shallow de-orbiting of the European Space Agency's (ESA) Automated Transfer Vehicle 5 (ATV-5), originally scheduled to take place in early 2015. Initial plans were made to undertake a joint trial between the United Kingdom and New Zealand in order to observe this event. Although the original re-entry scenario was subsequently altered by ESA, so that the event was not visible from New Zealand, the joint trial was conducted and a number of surrogate targets were observed using readily available, off-the-shelf equipment, such as CCD (charge coupled device) cameras fitted with standard photographic lenses. It was demonstrated that relatively inexpensive, portable equipment can be used to determine the position of a satellite in low Earth orbit (LEO) with an average precision of 10-15 metres in space [1].

After the initial success of the ATV-5 trial, a decision was made to continue building the SSA capability in New Zealand. DTA now operates a small SSA observatory located at Whangaparaoa Peninsula, just north of Auckland. The observatory has a 3-metre dome, equipped with a robotic tracking mount, a couple of 11-inch telescopes and a number of cooled CCD cameras. This gives us the ability to track smaller objects in LEO and GEO (geostationary Earth orbit). Currently, the observatory is undergoing a major modification to become a fully automated facility, for a significant increase in data collection efficiency.

Both astrometric and photometric observations are part of the DTA SSA programme. In addition, a specialised quadruple polarimetric camera (QuadCam) was recently built, using an approach devised in the UK at the Defence Science and Technology Laboratory (DSTL). Some modifications to the camera were made at DTA for improved performance. The initial results, based on observations of satellites in LEO, have demonstrated that the polarimetric signature of an object in space provides additional information that cannot be obtained from photometry alone [2].

At DTA we use our own software tool, *StarView* [1, 2], which has been developed specifically for automated astrometric and photometric analysis of images taken with our SSA equipment. The software is capable of fast and efficient astrometric calibration of images covering a range of field sizes, from under one degree to over 30 degrees in diameter. This has been achieved by optimising the image reduction algorithms to best match the sensor specifications.

It has been recognised that New Zealand has a unique geographic location in the South Pacific, which offers an opportunity to monitor satellite passes that cannot be observed from any other location. For example, many satellites scheduled for deorbiting often pass above New Zealand before entering the atmosphere over the Pacific Ocean. Having a robust SSA capability in New Zealand offers a possibility for international collaboration in this area. Given current priorities within DTA, our focus is placed on data collection and image analysis for specific satellites of interest to the NZDF and the wider operational community.

During the past few months, the focus has been mainly on photometric measurements of geostationary satellites over the Western Pacific, as part of collaboration with the Defence Research and Development Canada (DRDC). This paper provides a summary of some photometric observations and data analysis techniques, including a selection of sample light curves, in order to demonstrate the capability of the DTA SSA equipment.

2. OBSERVATIONS

All observations presented in this paper were made from the DTA SSA observatory near Auckland (36° 36.1′ S, 174° 50.1′ E), using an 11-inch Celestron EdgeHD Schmidt–Cassegrain telescope (SCT) at a focal ratio of f/10 (2800 mm focal length). The telescope is equipped with a Quantum Scientific Imaging (QSI) 640ws CCD camera, which is based on a Kodak KAI-04022 interline-transfer CCD chip with a resolution of 2048 × 2048 pixels. The pixel size is 7.4 μm, with a full well capacity of 40,000 electrons. The camera is cooled to −10 °C in order to reduce the thermal noise.

At the focal length of 2800 mm, the QSI camera covers a field of view of about one third of a degree (18.6′) on the side, or just less than half a degree (26.3′) on the diagonal. Using the same camera on the 11-inch f/2.2 Rowe-Ackermann Schmidt Astrograph (RASA) would have increased the field of view to about 2° diagonal, but it was found that using a longer focal length helps with isolating the satellite in images containing a large number of background stars, especially in crowded fields of the Milky Way.

A specialised GPS unit developed at DTA [1, 2] has been used for recording the time of observation to an accuracy of less than 1 ms. Although this level of accuracy is not normally required for photometric observations of geostationary satellites, due to relatively long exposure times involved, the provision has been made to use the same images for astrometric measurements at a later stage.

Six geostationary satellites positioned over the Western Pacific Region have been selected for this study in order to test the performance of the equipment and data reduction procedures. The satellites are listed in Table 1. They are all located relatively close to each other, spreading over about two degrees in the sky, which makes them very convenient to observe and compare. The first five satellites (Express-AT2, Express-AM5, Sky Muster, Himawari-8 and Himawari-9) form a very tight cluster measuring only 1° in the sky. The last satellite, Apstar-9, is located about 1° further to the east. The group represents a combination of telecommunication and weather satellites, based on a variety of different buses, which are expected to give different photometric signatures.

The centroid of the satellite group is located roughly at a longitude of 141° E. The view from this point in the geostationary orbit, from an altitude of 35,786 km, is shown in the left panel of Fig. 1. The view is centred over the

easternmost parts of Indonesia, just off the cost of New Guinea. When viewed from Auckland, New Zealand, the satellite group is seen between 34° and 35°above the north-western horizon, as shown in the right panel of Fig. 1.

The observations presented in this paper were made on the night of 6th August 2018. The telescope mount was programmed to cycle through five positions in the sky in order to cover every satellite from the list (the Himawari-8 and Himawari-9 were captured in one frame, as they are only 0.1° apart), while the exposure duration was fixed at 20 seconds. The cycle was repeated every 3 minutes in average. A total of 900 images were collected (180 frames per satellite) over the period of about 9 hours.

Table 1. Satellite list

Satellite name	*NORAD*	*COSPAR*	*Country*	*Description*	*Longitude*	*Bus type*
Express-AT2	39613	2014-010B	Russia	Communications	139.9° E	Express-1000K
Express-AM5	39487	2013-077A	Russia	Communications	140.0° E	Express-2000
Sky Muster (NBN1A)	40940	2015-054A	Australia	Communications	140.2° E	SSL-1300
Himawari-8	40267	2014-060A	Japan	Weather	140.7° E	DS-2000
Himawari-9	41836	2016-064A	Japan	Weather	140.8° E	DS-2000
Apstar-9	40982	2015-059A	China	Communications	142.0° E	DFH-4

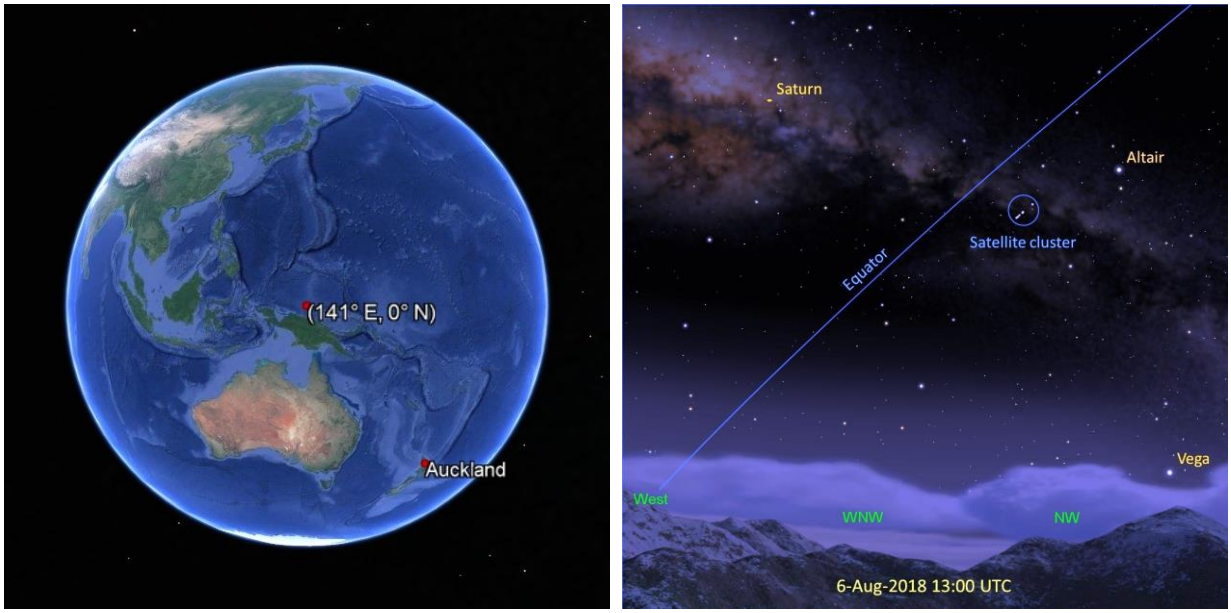

Fig.1. Left: Earth view from the centroid of the satellite group at a longitude of 141° E. Right: The satellite group in the sky, as seen from the DTA SSA Observatory, Auckland, New Zealand (the satellite brightness is largely exaggerated).

The images were taken with the sidereal tracking turned off. In this case, any geostationary satellite appears as a well-defined point source, while the stars leave parallel streaks. The length of the streaks is directly proportional to the exposure duration. While having a longer exposure reduces the noise in satellite photometry, it makes the astrometric analysis considerably harder, as the background stars are used for calibration purposes. Also, longer stellar streaks increase the risk of some of the stars passing right through the satellite image, therefore making it virtually impossible to measure the satellite flux.

Two examples of a satellite images are shown in Fig. 2, both taken at around 13:24 UTC, as the satellite group was exiting the Milky Way. South is on the left and east is on the top. The camera is oriented so that the stars enter the image at the top and leave at the bottom, creating vertical traces, while the declination axis is roughly horizontal. The left panel of Fig. 2 shows Himawari-8 and Himawari-9, almost at the same declination (horizontal axis) and

separated by about 650 pixels or 365 arc seconds along the right ascension (vertical axis). This is in good agreement with the satellite longitude difference of 0.1° found from Table 1. Both satellites show the same brightness of about 11.4 magnitudes. The right panel of Fig. 2 shows Apstar-9, recorded half a minute later at a magnitude of 10.3.

In order to calibrate the satellite measurements, a number of images of stars were recorded during the same observation night, and keeping the telescope at the same position in the sky, but with the sidereal tracking turned on. An example of a star field is shown in Fig. 3, together with an illustration of the star identification process (as explained in the next section). The image is roughly centred on a 10-magnitude star GSC 439-511 (the corresponding Tycho catalogue number is 439-511-1).

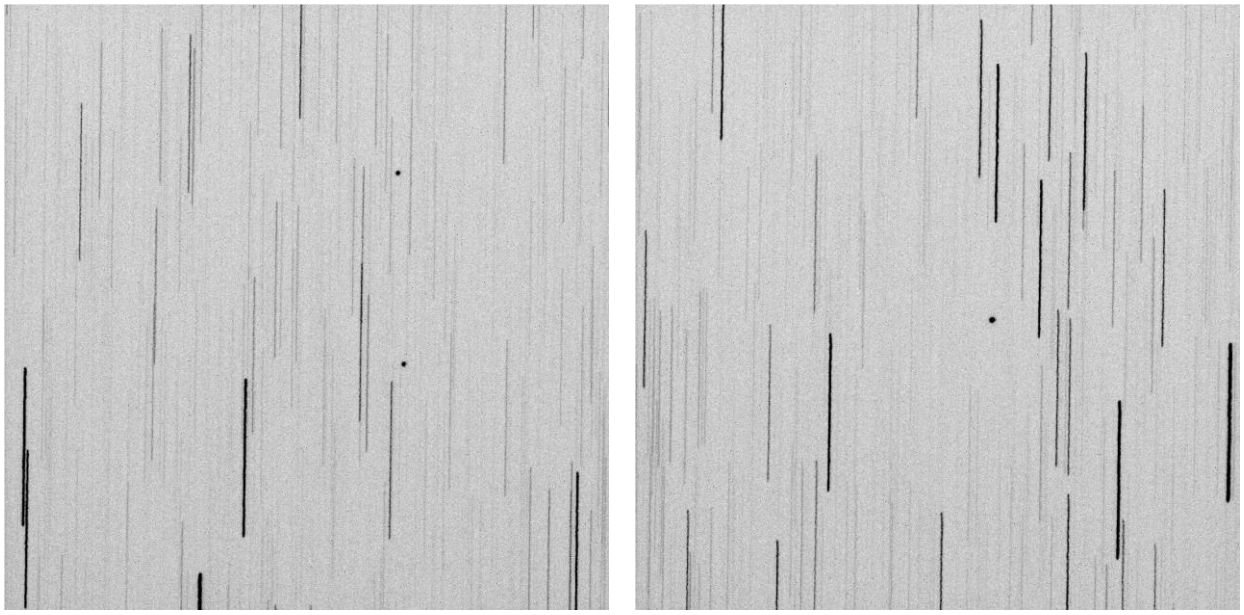

Fig 2. Left: Himawari-8 (bottom) and Himawari-9 (top) at 13:24:12 UTC. Right: Apstar-9 at 13:24:42 UTC

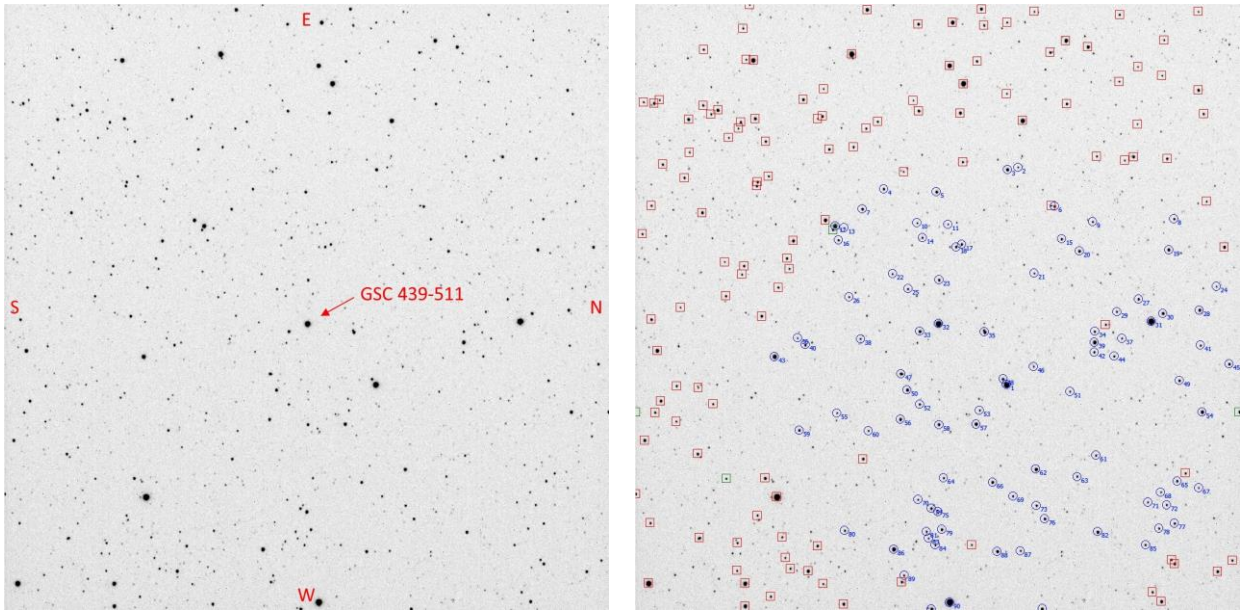

Fig. 3. Left: Star field around GSC 439-511. Right: An illustration of the star detection and identification process.

3. DATA REDUCTION

The astrometric and photometric calibration of all stellar fields was performed using *StarView*, a software tool developed at DTA for the reduction of SSA data [1, 2]. The process of star detection and identification is illustrated in the right panel of Fig. 3. All stars detected above a given intensity threshold are marked as red squares. A special algorithm developed at DTA called *stellar fingerprints* [1] is then used to recognize the stellar field and select a subset of reference stars, marked as blue circles. As a final step (not shown in Fig. 3), all remaining stars in the image are cross-referenced with the catalogue and the star identification process is complete. We use *Gaia* Data Release 1 [3, 4] for both astrometric and photometric calibrations. Our software is currently being modified to include *Gaia* Data Release 2, which is the latest release of the catalogue [5].

In the example above, about 200 stars have been detected as well defined point sources. About half of those were identified as reference stars (blue circles) in the first pass of the calibration algorithm. The remaining stars were then identified in the second pass. Only about 10 stars were not found in the catalogue, as they were below the selected magnitude limit. The astrometric solution was obtained as a two-dimensional polynomial fit of relatively low order of $n = 3$ in both axes. A typical uncertainty of the fit was around 0.1 arc seconds.

The photometric calibration is performed based on the *Gaia* G-band magnitudes. The stellar fluxes are obtained by integrating the pixel values over a circular aperture with a radius of 12 pixels, centred on each star. Additional four pixels around the aperture are used to estimate the median background level. The plot of magnitude versus flux (on a logarithmic scale) is shown in Fig. 4. As expected, the calibration is linear, with a slope close to −2.5, in agreement with Pogson's formula.

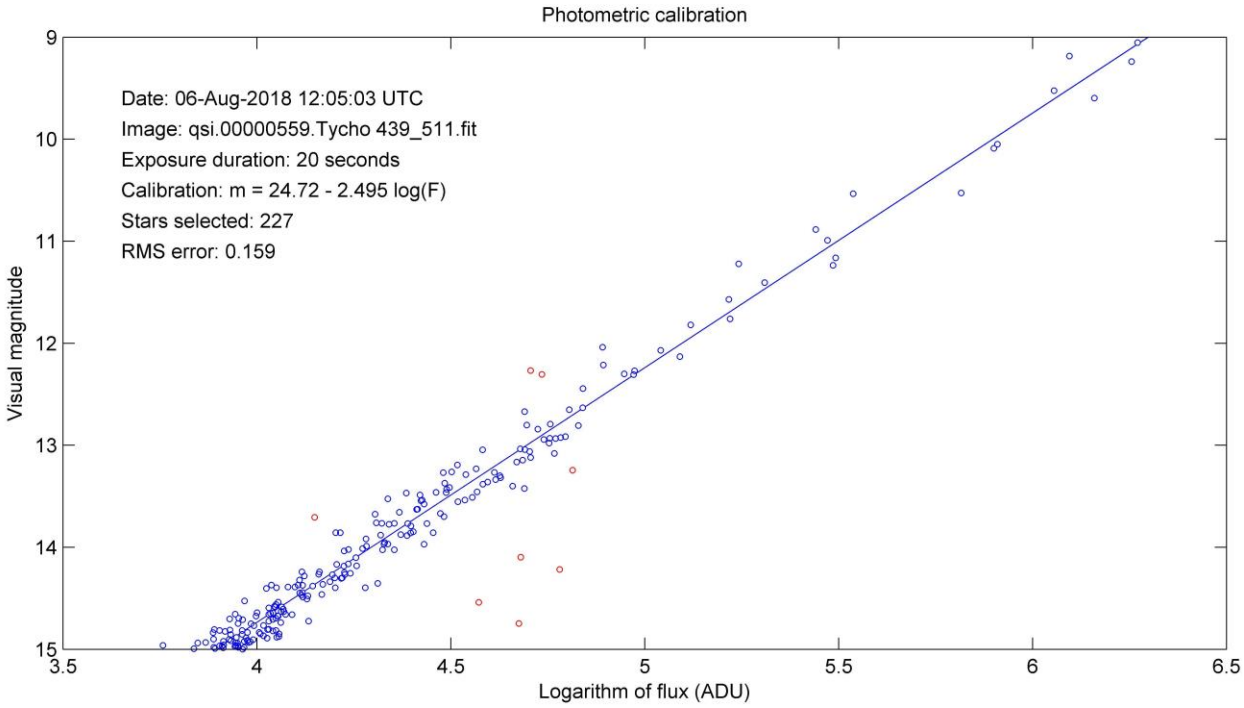

Fig. 4. Photometric calibration

Instead of computing a complete linear fit through the calibration points, it is often assumed that the slope of the calibration line is exactly −2.5 (theoretical value), and only the zero point is obtained from the data [6]. In the case of a perfectly linear CCD detector, both methods will produce exactly the same results. By doing a full linear fit, however, the linearity of the detector can easily be checked.

A typical root-mean-square (RMS) error of the photometric calibration fit from our star fields is about 0.1 magnitudes. Most of the scatter around the best fit is caused by stellar colours, as we do not use any photometric filters in our observations. This is a common situation in satellite photometry [6] and does not affect the results, as long as the focus is on monitoring relative variations in satellite brightness. In situations where high-precision photometry is required, a set of proper photometric filters can be used [7, 8].

4. PHASE ANGLE CONSIDERATIONS

Once the visual magnitudes for a satellite are computed from observations, the resulting light curve is usually plotted as a function of the phase angle (φ), which is defined as the angle between the Sun, satellite and observer, as illustrated in Fig. 5. The phase angle is normally calculated from the scalar product: $\cos\varphi = \vec{l}_{\text{sun}} \cdot \vec{l}_{\text{obs}}$, where $\vec{l}_{\text{sun}}$ and $\vec{l}_{\text{obs}}$ are unit vectors defining the viewing directions from the satellite towards the sun and observer, respectively [6]. The satellite normally appears the brightest at a phase angle of zero degrees, when the geometry resembles that of a full Moon, or a planet at opposition. By convention, the phase angle is usually considered negative before the opposition (while the angle is closing) and positive afterwards (as the phase angle is opening). This ensures a smooth transition of the phase angle around the point of opposition, as this is normally observed during the night. The total span of values is therefore between −180° and +180°, where the extreme values of ±180° occur during the daylight and are not normally observed.

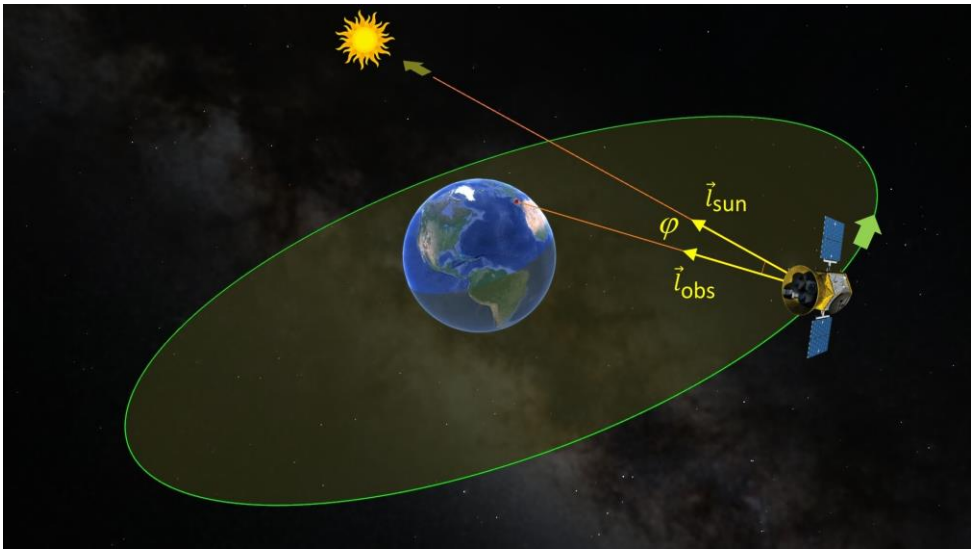

Fig. 5. Phase angle

Plotting a satellite light curve as a function of phase angle has the advantage of providing the relative position of the Sun in the same plot. However, this does not always work well close to the point of opposition, unless the satellite, observer and Sun are perfectly aligned. To illustrate this, let us assume that the Sun is high above the equatorial plane (for example during the time of solstice), and the observer is on the opposite hemisphere (a typical winter situation). In this case, the phase angle around the opposition will never reach zero degrees. The minimum value can be as high as 30° for an observer at mid-latitudes. This means that the phase angle will jump abruptly from –30° to +30°, leaving a large gap in the light curve. In addition, the data will appear unnaturally compressed and distorted immediately before and after the two points of discontinuity, as the phase angle will change very slowly while passing through the minimum.

In order to avoid these difficulties, we use the projection of the phase angle onto the equatorial plane, as illustrated in Fig. 6. The equatorial phase angle depends only on the right ascension of the Sun and satellite and can be calculated as $\varphi_{\text{eq}} = 180° - \Delta\alpha$, where $\Delta\alpha$ is the difference in right ascension between the Sun and the satellite

($\Delta\alpha = \alpha_{\text{sun}} - \alpha_{\text{sat}}$). If $\Delta\alpha$ is always kept in the range between 0° and 360°, then the equatorial phase angle will remain between −180° and +180°, in agreement with the sign convention introduced earlier. In other words, the phase will be negative when closing (i.e. before the opposition) and positive when opening (after the opposition). Defined in this way, the equatorial phase angle is practically a linear function of time and will always pass through zero degrees when the satellite is at opposition, making it very suitable as a replacement for the time axis.

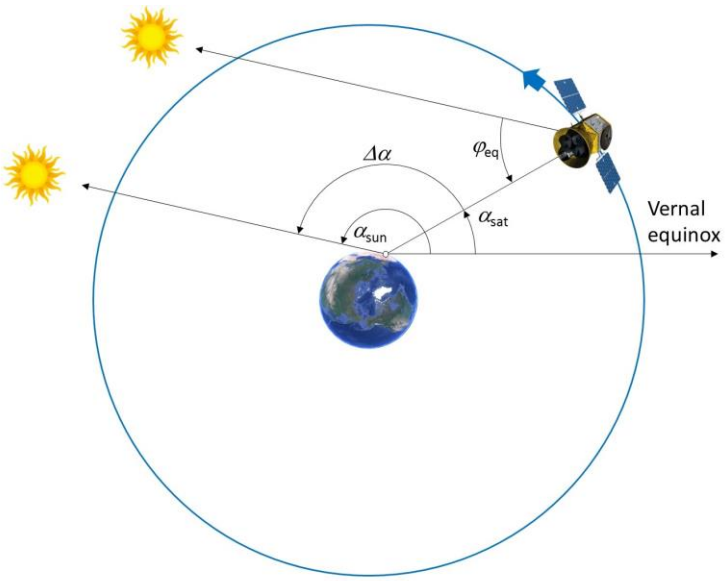

Fig. 6. Equatorial phase angle

5. RESULTS

The light curves for all six satellites from Table 1 are shown in Fig. 7. The visual magnitude is plotted as a function of the equatorial phase angle, as described above. In general, all satellites show smooth variation in brightness that increases gradually as the satellite approaches the opposition (phase angle of zero degrees). Occasional glints have been recorded as a result of specular reflection off flat surfaces. A typical random error obtained from the smooth sections in the light curves is less than 0.01 magnitudes. The overall change in brightness for some satellites (such as Express-AT2) spans almost five magnitudes, which corresponds to a flux ratio of 100.

Several satellites plotted in Fig. 7 show a distinct flattening of the light curve, i.e. roughly constant brightness at phase angles larger than about −100° to −80°. This is due to the fact that satellites at large phase angles are largely illuminated not by the direct sun light, but by the light reflected from the Earth. A simple photometric model [9, 10] can be used to explain this behaviour.

It is also interesting to compare the light curves of Himawari-8 and Himawari-9. They are two identical satellites, based on the same bus DS-2000 (see Table 1). However, while the two light curves are mainly indistinguishable between −70° and −15°, Himawari-9 shows a bright, rather broad glint of about two magnitudes above the base level centred at about −90°, while Himawari-8 appears much brighter at the opposition (0°), when the main glint from the solar panels is expected. This might mean that the solar panels on Himawari-9 are still not aligned. The satellite was launched in 2016, but is currently on standby until 2022, when it will replace Himawari-8.

Most light curves appear symmetrical around the zero point, with some features mirror imaged around the line $\varphi = 0°$ (for example the close pairs of minor peaks seen in Express-AM5 and Sky Muster), but this behaviour is not always observed in geostationary satellites, as it depends on many parameters, such as the satellite bus characteristics and illumination geometry [6].

Another interesting comparison can be made between the light curves of Express-AT2 and Express-AM5. Although both satellites belong to the same series, they are not based on the same bus. Express-AM5 is a 3-ton satellite, much bigger (and brighter) than Express-AT2, weighing only about a ton. The two light curves show a distinct difference of about 1.5 magnitudes over the entire range of phase angles. This is a nice example of two satellites that can easily be distinguished by their brightness, in situations where positional data are not available. This method has been used in the past to correct some misidentification errors between satellites in the geostationary belt [6].

Finally, we should note that the light curve of Apstar-9 also shows a prominent peak of about 1.5 magnitudes above the base level at a phase angle of –60°, which might mean that the solar panels are not facing the sun (similar to Himawari-9 above).

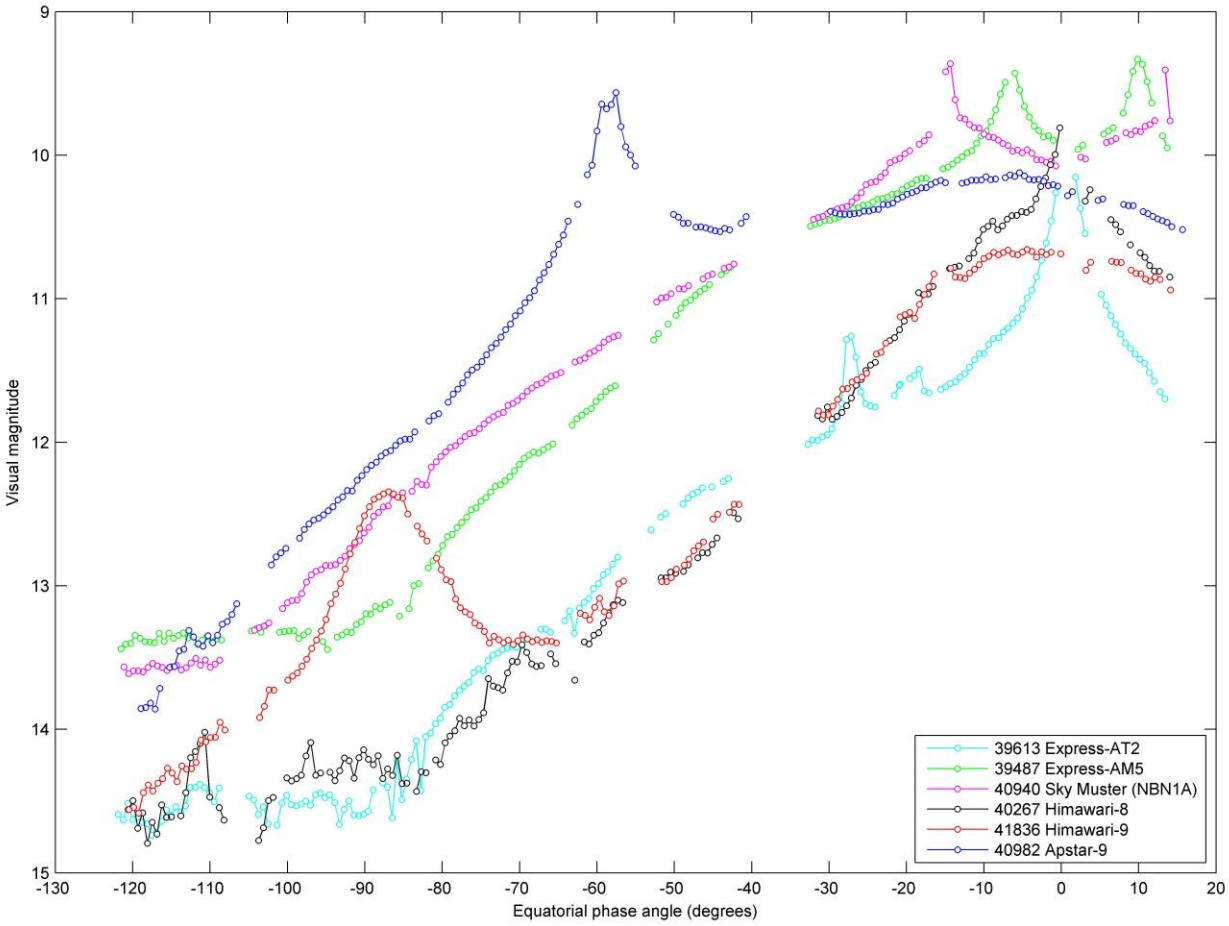

Fig. 7. Light curves of the six target satellites from Table 1.

6. SUMMARY

The Defence Technology Agency, of the New Zealand Defence Force, has steadily been increasing its space situational awareness capability. The recent focus has been on the photometric measurements of geostationary satellites using the DTA 11-inch Schmidt-Cassegrain telescope and a Quantum Scientific Imaging CCD camera. Six geostationary satellites over the Western Pacific Region were selected within a narrow range of longitudes between 140° E and 142° E, to test the equipment and data analysis techniques. The observations were made on the night of 6th August 2018, covering about nine hours of continuous photometry. The moment of opposition with the Sun (the equatorial phase angle of zero degrees) was recorded in all light curves towards the end of the night.

The images were analysed using the DTA-developed software, *StarView*. The photometric calibration was based on the European Space Agency's *Gaia* catalogue (Data Release 1). This gives a typical uncertainty in absolute photometry of about 0.1 magnitudes, while any random errors in satellite photometry between consecutive images were found to be less than 0.01. The limiting magnitude of our optical system is about 15-16.

The light curves of the satellites included in this study generally show a typical smooth increase in brightness as the phase angle closes towards the opposition with the Sun. Occasional glints (specular reflections) have been recorded at high phase angles on some satellites, possibly indicating a misalignment of the main solar array. It was demonstrated that this type of measurements can be used to distinguish between satellites based on a different bus, or to detect any difference in orientation between satellites based on the same bus.

7. ACKNOWLEDGEMENTS

This work has made use of data from the European Space Agency (ESA) mission *Gaia* (https://www.cosmos.esa.int/gaia), processed by the *Gaia* Data Processing and Analysis Consortium (DPAC, https://www.cosmos.esa.int/web/gaia/dpac/consortium). Funding for the DPAC has been provided by national institutions, in particular the institutions participating in the *Gaia* Multilateral Agreement.

8. REFERENCES

1 Skuljan, J. and Kay, J., Automated astrometric analysis of satellite observations using wide-field imaging, *Proc. 17th AMOS Conf.,* pp. 240-249, 2016

2 Skuljan, J., QuadCam – a quadruple polarimetric camera for space situational awareness, *Proc. 18th AMOS Conf.,* pp. 275-285, 2017

3 Gaia Collaboration, Prusti, T., de Bruijne, J. H. J., Brown, A. G. A., Vallenari, A., Babusiaux, C., Bailer-Jones, C. A. L., Bastian, U., Biermann, M., Evans, D. W., et al., The Gaia mission, *A&A*, 595, pp. A1, 2016

4 Gaia Collaboration, Brown, A. G. A., Vallenari, A., Prusti, T., de Bruijne, J. H. J., Mignard, F., Drimmel, R., Babusiaux, C., Bailer-Jones, C. A. L., Bastian U., et al., Gaia Data Release 1. Summary of the astrometric, photometric, and survey properties, *A&A*, 595, pp. A2, 2016

5 Gaia Collaboration, Brown, A. G. A., Vallenari, A., Prusti, T., de Bruijne, J. H. J., Babusiaux, C. and Bailer-Jones, C. A. L. , Gaia Data Release 2. Summary of the contents and survey properties, *ArXiv e-prints*, 2018

6 Scott, R. and Wallace, B., Small-aperture optical photometry of Canadian geostationary satellites, *Can. Aeronaut. Space J.*, Vol. 55, No. 2, pp. 41-53, 2009

7 Jolley, A., Analysis of specular reflections off geostationary satellites, *Proc. 17th AMOS Conf.,* pp. 1096-1105, 2016

8 Schmitt, H. R., Vrba, F. J., Multicolor observations of geostationary satellites, *Proc. 17th AMOS Conf.,* pp. 1367-1370, 2016

9 Cognion, R. L., Observations and modeling of GEO satellites at large phase angles, *Proc. 14th AMOS Conf.,* 2013

10 Davies, D.W., Simplified photometric model of a GeoSat with earthshine, *Aerospace Report* ATR-2012(8480)-1, Contract No. FA8802-09-C-001, 2012